Inorganic Chemistry
Article

Inorg. Chem. **2009**, *48*, 11691–11696 **11691**
DOI: 10.1021/ic901735d

$La_{1-x}Ce_xCrO_3$ ($0.0 \leq x \leq 1.0$): A New Series of Solid Solutions with Tunable Magnetic and Optical Properties

Rakesh Shukla,[†] Jayappa Manjanna,[†] Anup K. Bera,[‡] Seikh M. Yusuf,[‡] and Avesh K. Tyagi*[,†]

[†]*Chemistry Division and* [‡]*Solid State Physics Division, Bhabha Atomic Research Centre, Mumbai − 400 085, India*

Received September 1, 2009

A new series of $La_{1-x}Ce_xCrO_3$ ($0.0 \leq x \leq 1.0$) compounds in nanocrystalline form were synthesized using a two-step synthesis route, involving an initial combustion reaction followed by vacuum heating in the presence of a Zr sponge, which acted as an oxygen getter. For the first time, a homogeneous solid solution formation throughout the entire range was obtained in this series. These compounds were characterized using X-ray diffraction, diffuse reflectance UV visible spectrophotometry, and superconducting quantum interference device magnetometry. The crystallite size for the phase-pure products was confirmed to be ~42−44 nm by high-resolution transmission electron microscopy. All compounds (nanocrystalline) in this series are found to be predominantly antiferromagnetic in nature with a remarkable linear increasing trend in Neel temperature from 257 to 281.5 K as a function of decreasing Ce^{3+} content. Interestingly, the band gap also shows a linear decrease from 3.21 to 3.02 eV as a function of increasing Ce^{3+} concentration in the $La_{1-x}Ce_xCrO_3$ series.

Introduction

Perovskites are an interesting class of materials with a variety of properties attractive for potential applications such as use as catalysts, high-temperature electrodes, thermoelectric materials, and more recently biferroic materials.[1−4] Rare earth chromates belong to the perovskite family, where Cr^{3+} is present at B-sites, and any of the rare earth ions (La^{3+}−Lu^{3+}) at A-sites, such perovskite type ($RECrO_3$), are technologically important as well, as lighter rare earth chromates are used as interconnects in solid oxide fuel cells and heavier ones have recently joined the important class of multiferroics.[5]

$LaCrO_3$, is a perovskite-type material which has an orthorhombic $GdFeO_3$-type crystal structure at room temperature, with space group *Pbnm*[6,7] and lattice parmeters[8] $a = 5.477$ Å, $b = 5.514$ Å, and $c = 7.755$ Å. The magnetic ordering in $LaCrO_3$ is G-type antiferromagnetic ($T_N = 282$ K),[9] wherein a $Cr^{3+}(3d^3{:}t_{2g}^3e_g^0)$ moment is antiferromagnetically coupled with all six of its nearest-neighbors Cr^{3+} moments. Several studies are available in the literature[10−13] on its magnetization at various temperatures after doping by trivalent and divalent ions at the La site [La^{3+} ($4f^0$): closed-shell with no f electron]. Some of these studies showed a limited solubility of the guest ions in the structure of $LaCrO_3$. Since Ce^{3+} has one unpaired electron in the 4f shell, the magnetic and optical properties of Ce^{3+}-doped $LaCrO_3$ compounds will be of great interest as a function of Ce^{3+} content in the lattice of $LaCrO_3$. The preparation of Ce^{3+}-substituted $LaCrO_3$ is extremely unfavorable, as most of the time the products formed are biphasic, due to the phase separation of CeO_2, driven by the oxidation of Ce^{3+}. Thus, the synthesis of Ce^{3+}-doped $LaCrO_3$ is a challenging task. Up until now, there has been only one study on the solubility of the Ce^{3+} ($4f^1$) ion in $LaCrO_3$, by Winkler et al.,[14] wherein a maximum solubility of up to 20% Ce^{3+} was achieved by a solid-state route. In light of the very close ionic sizes of La^{3+} and Ce^{3+} (the ionic

*To whom correspondence should be addressed. Phone: +91-22-25595330. Fax: +91-22-25505151. E-mail: aktyagi@barc.gov.in.

(1) Moreira dos Santos, A.; Cheetham, A. K.; Atou, T; Syono, Y.; Yamaguchi, Y.; Ohoyama, K.; Chiba, H.; Rao, C. N. R. *Phys. Rev. B* **2002**, *66*, 064425.
(2) Kimura, T.; Kawamoto, S.; Yamada, I.; Azuma, M.; Takano, M.; Tokura, Y. *Phys. Rev. B* **2003**, *67*, 180401.
(3) Sosnowska, I.; Peterlin-Neumaier, T; Steichele, E. *J. Phys. Chem.* **1982**, *15*, 4835.
(4) Niitaka, S.; Azuma, M.; Takano, M.; Nishibori, E.; Takata, M.; Sakata, M. *Solid State Ionics* **2004**, *172*, 557.
(5) Serrao, C. R.; Kundu, A. K.; Krupanidhi, S. B.; Waghmare, U. V.; Rao, C. N. R. *Phys. Rev. B* **2005**, *72*, 220101.
(6) Geller, S. *J. Chem. Phys.* **1956**, *24*, 1236.
(7) Geller, S. *Acta Crystallogr.* **1957**, *10*, 243.
(8) Geller, S.; Raccah, P. M. *Phys. Rev. B* **1970**, *2*, 1167.
(9) Bertaut, E. F.; Mareschal, J.; Vries, G. De.; Aleonard, R.; Pauthenet, R.; Rebouillat, J. P.; Zarubicka, V. *IEEE Trans. Magn.* **1966**, *2*, 453.
(10) Bents, U. H. *Phys. Rev. B* **1957**, *106*, 225.
(11) Goodenough, J. B. *Magnetism and the Chemical Bond*; John Wiley & Sons: New York, 1963; p 100.
(12) Arakawa, T.; Tsuchi-ya, S.; Shiokawa, J. *Mater. Res. Bull.* **1981**, *16*, 7.
(13) Chakraborty, K. R.; Das, A.; Yusuf, S. M.; Krishna, P. S. R.; Tyagi, A. K. *J. Magn. Magn. Mater.* **2006**, *301*, 74.
(14) Winkler, E.; Causa, M. T.; Neumeier, J. J.; Oseroff, S. B. *J. Magn. Magn. Mater.* **2007**, *310*, e959–e961.

Published on Web 11/17/2009

radii of La^{3+} and Ce^{3+} are 1.03 Å and 1.01 Å, respectively), there is no reason that a wide solubility of Ce^{3+} in $LaCrO_3$ should not exist, except for the lack of a favorable synthesis route. In order to overcome the variable oxidation state limitation, we have developed a two-step process to synthesize the $La_{1-x}Ce_xCrO_3$ ($0.0 \le x \le 1.0$) series for the first time. The optimized synthesis condition could yield an ideal homogeneous solid solution over the entire ($0.0 \le x \le 1.0$) range in the $La_{1-x}Ce_xCrO_3$ series. Samples in the $La_{1-x}Ce_xCrO_3$ series were characterized in detail. The structural, magnetic, and optical properties of all compositions in the series have been studied, and the results are presented in the manuscript. All of these results support the formation of solid solutions in this series of oxides. A close correlation between structure, different physical properties, and the Ce^{3+} content is conducted in the study.

Experimental Section

All of the samples in the $La_{1-x}Ce_xCrO_3$ ($0.0 \le x \le 1.0$) series were synthesized using a two-step synthesis route.[15] In the first step, a stoichiometric amount of lanthanum oxide (La_2O_3), cerium nitrate ($Ce(NO_3)_3 \cdot 6H_2O$), and chromium nitrate ($Cr(NO_3)_3 \cdot 9H_2O$) were mixed together and dissolved in a minimum volume of nitric acid to obtain the mixed metal nitrate solution. On the basis of the stoichiometric ratio concept,[16] the ratio of oxidizing and reducing valencies should be unity, which leads to the maximum exothermicity. In the present case, a stoichiometric ratio (1:3.33) of total nitrates and fuel (glycine) was selected. A stoichiometric amount of glycine was added to the mixed metal nitrate solution in each case. The as-prepared fuel−nitrate solution was heated up slowly on a hot plate to produce a deep green viscous gel. On further heating, the gel swelled and was autoignited to produce a voluminous gray-greenish powder. In the second step, the combustion products were pelletized and wrapped in a tantalum foil, which were placed in a quartz tube along with a Zr sponge without any physical contact. The quartz tube was evacuated to 10^{-5} mbar and sealed online. These ampules were then heated at 1000 °C for 12 h. The X-ray diffraction (XRD) data were recorded with a PANalytical (X'pert PRO) X-ray diffractometer using Ni-filtered Cu K_α radiation. Silicon was used as an external standard for the correction of the instrumental broadening. The diffraction data were analyzed using the Rietveld method using the Fullprof-2K software package.[17] In order to study the morphology of the samples, transmission electron microscopy (TEM) investigations were carried out using a Philips CM30/Super TWIN Electron Microscope. A diffuse reflectance (DR)−UV−visible spectrophotometer was used in the reflectance mode for investigating optical properties. The magnetic measurements were carried out using a Quantum Design MPMS-XL superconducting quantum interference device magnetometer. Magnetization (M) as a function of temperature (T) was measured under zero-field-cooled (ZFC) and field-cooled (FC) modes over a temperature range of 5−300 K. In ZFC mode, the sample was first cooled down to 5 K in the absence of any external magnetic field, and then an external field was turned on at 5 K (ca. H = 500 Oe) to measure M during warming of the sample up to 300 K. In FC mode, the M was measured while cooling the sample back to ca. 5 K under the same applied field H (500 Oe). Also, M versus H was measured up to a field of 50 kOe at 300 K for all of the samples for a single quadrant and at 200 K up to the maximum field of 10 kOe over all four quadrants.

Results and Discussion

In our initial attempts, we tried to synthesize the $La_{1-x}Ce_xCrO_3$ ($0.0 \le x \le 1.0$) series using a conventional solid-state method in a reducing atmosphere, but a biphasic product consisting of $LaCrO_3$ and $CeCrO_3$ was obtained, attributed to the difference in the kinetics of formation of these two individual phases. In the solid-state reaction, when the well-mixed reactants La_2O_3, CeO_2, and Cr_2O_3 were heated in a vacuum-sealed quartz tube in the presence of a zirconium sponge, La_2O_3 reacted faster with Cr_2O_3 to form $LaCrO_3$, while $CeCrO_3$ was formed only after the reduction of CeO_2 to Ce_2O_3 followed by its reaction with Cr_2O_3. This sequential reaction led to a biphasic product consisting of $LaCrO_3$ and $CeCrO_3$. The identification of the two phases by XRD was rather difficult due to similar values of cell parameters of $LaCrO_3$ and $CeCrO_3$. However, the presence of these two phases would be ascertained by the temperature-dependent magnetization [$M(T)$] study, which showed two distinct Néel temperatures (T_N) corresponding to $LaCrO_3$ (282 K) and $CeCrO_3$ (257 K).

Since the synthesis of this series using a solid-state method failed, it was required to develop a process in which a Ce^{3+}-based precursor could be used. For this purpose, one of the best-suited synthesis methods is the combustion technique, which produces ultrafine powders of ceramics in a shorter time and with improved powder characteristics. A major advantage of this method is intimate blending among the constituents using a suitable fuel in an aqueous medium.[16,18] Glycine is one of the most efficient fuels which gives maximum exothermicity under stoichiometric conditions; hence, a glycine−nitrate combustion reaction was used for the preparation of the series. It was observed that, during the autoignition process, a large amount of evolved gases dissipates the heat and minimizes the local sintering, making the powders highly porous and frothy. The products obtained after combustion were wrapped in tantalum foil and heated in a vacuum-sealed quartz tube at 1000 °C in the presence of a zirconium sponge for 12 h. Zr sponge was used to remove any excess oxygen from the product and carbonaceous impurities, if any. Zr sponge reduces the partial pressure of oxygen, so as to prevent the phase separation of $La_{1-x}Ce_xCrO_3$ to $LaCrO_3$ and CeO_2, due to the oxidation of Ce^{3+} to Ce^{4+}. XRD patterns of all samples were qualitatively similar to that of $LaCrO_3$, with a slight shift of Bragg peak positions toward the higher angles. Typical Rietveld refinement plots of X-ray diffraction data for x = 0.1, 0.5, and 0.9 samples are shown in Figure 1. The Rietveld analysis reveals that all samples crystallize in the orthorhombic crystal structure with the space group *Pbnm* (no. 62). The crystal structures for all samples conceive a distorted perovskite-type structure. A schematic representation of the crystal structure for the perovskite-type lattice of $La_{1-x}Ce_xCrO_3$ is shown in Figure 2. The refined unit cell parameters for all of the studied compounds are listed in the Table 1, which indicates a gradual decrease in a and c parameters with the increase of Ce concentration, whereas parameter b remains almost

(15) Shukla, R.; Bera, A. K.; Yusuf, S. M.; Deshpande, S. K.; Tyagi, A. K.; Hermes, W.; Eul, M.; Pöttgen, R. *J. Phys. Chem. C* **2009**, *113*, 12663.
(16) Bedekar, V.; Shukla, R.; Tyagi, A. K. *Nanotechnology* **2007**, *18*, 155706.
(17) Roisnel, T.; Rodriguez-Carvajal, J. *FULLPROF 2008: A Program for Rietveld, Profile Matching and Integrated Intensity Refinements for X-ray and Neutron Data*; LCSIM: Rennes, France, 2008.
(18) Deganello, F.; Marcì, G.; Deganello, G. *J. Eur. Ceram. Soc.* **2009**, *29*, 439.

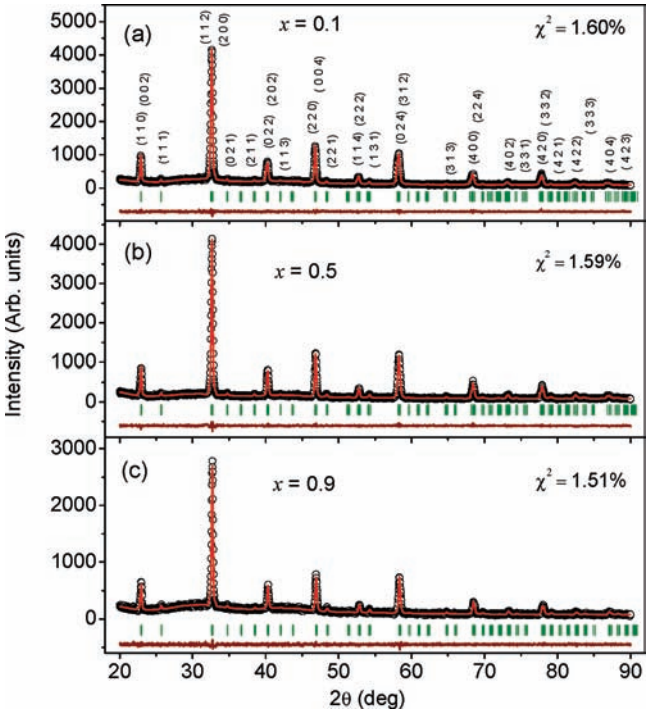

Figure 1. Rietveld refined XRD patterns of (a) $La_{0.9}Ce_{0.1}CrO_3$, (b) $La_{0.5}Ce_{0.5}CrO_3$, and (c) $Ce_{01}Cr_{0.9}O_3$ compounds. The observed and calculated patterns are denoted by open circles and solid lines. The solid lines at the bottom of the each panel show the difference patterns. The Bragg peak positions are marked by vertical lines. The *hkl* values for the observed peaks are also listed.

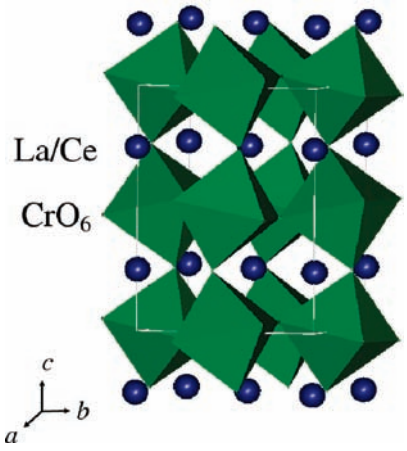

Figure 2. Schematic representation of the crystal structure for $La_{1-x}Ce_xCrO_3$.

constant throughout the homogeneity range. The Rietveld refined atomic positions, isotropic thermal parameters, and different agreement factors for $La_{1-x}Ce_xCrO_3$ ($0.0 \le x \le 1.0$) are shown as Supporting Information. The change in the lattice parameters results in a linear decrease of the unit cell volume from 233.97(4) Å^3 for $x = 0.1$ to 231.95(4) Å^3 for $x = 1.0$. Thus, $LaCrO_3$ and $CeCrO_3$ form a solid solution throughout the range (further evidenced from magnetic and optical measurements, as discussed subsequently), which has been achieved for the first time. The decrease in the observed unit cell volume is additional evidence of Ce and Cr ions being in the +3 oxidation state. If cerium was in the +4 oxidation state in the perovskite lattice, then for charge neutrality the Cr ion should have been in the +2 oxidation state, which would have resulted in an expansion in the unit cell volume. The average crystallite size of these oxides obtained from the observed XRD line broadening (i.e., using the Scherrer equation: thickness, $t = 0.9\,\lambda/(B\cos\theta)$) was found to be in the range of 42−44 nm. In order to further confirm this, a representative sample, namely, $La_{0.5}Ce_{0.5}CrO_3$, was analyzed by high-resolution (HR)-TEM (Figure 3). The nanocrystalline nature of the sample is evident, although some extent of agglomeration is seen (Figure 3a), and the shape of the particles is almost regular (Figure 3b). The HR-TEM micrograph (Figure 3c) clearly shows the regularly arranged lattice fringes with no structural defects.

Table 1. Refined Lattice Parameters and Unit Cell Volumes for $La_{1-x}Ce_xCrO_3$ ($0.0 \le x \le 1.0$)[a]

Ce concentration (x)	a (Å)	b (Å)	c (Å)	V (Å^3)
0.1	5.5100(5)	5.4762(5)	7.7542(7)	233.97(4)
0.2	5.5079(5)	5.4763(6)	7.7516(8)	233.81(4)
0.3	5.5057(9)	5.4751(9)	7.7496(12)	233.61(6)
0.4	5.5026(6)	5.4752(6)	7.7477(8)	233.42(4)
0.5	5.4981(5)	5.4752(5)	7.7471(7)	233.21(4)
0.6	5.4964(6)	5.4749(6)	7.7451(8)	233.07(4)
0.7	5.4946(5)	5.4736(6)	7.7390(8)	232.73(4)
0.8	5.4882(4)	5.4745(5)	7.7383 (6)	232.50(3)
0.9	5.4863(7)	5.4748 (8)	7.7370(10)	232.37(5)
1.0	5.4801(5)	5.4738(5)	7.7324(6)	231.95(4)

[a] Orthorhombic crystal structure, space group: *Pbnm*.

Recently, we reported the preparation and magnetic behavior of $CeCrO_3$.[15] The temperature-dependent ZFC and FC magnetization curves for the samples of $La_{1-x}Ce_xCrO_3$ ($x = 0.1-1.0$) under the applied magnetic field of 500 Oe (Figure 4) show highly unusual magnetic behavior. The ZFC magnetization curves for all of the samples show a peak (for example, at 281.5 K for the $x = 0.1$ composition) with a lowering of the temperature which is attributed to the antiferromagnetic (AFM) ordering of the Cr^{3+} spins. Interestingly, the Neel temperature shifts linearly from 281.5 to 257 K with an increase of Ce^{3+} concentration from 0.1 to 1.0 (Figure 4). Upon further cooling, a slight increase in the ZFC magnetization has been observed below ~80−100 K for all samples. This increase in the magnetization can be attributed to the ordering of the Ce^{3+} spins as the magnetization at the lower temperatures increases with the increase of Ce^{3+} concentration. Remarkably, the temperature-dependent FC magnetization curves show different behavior as compared to that of the ZFC magnetization curves. Also, there is remarkable variation in the FC magnetization curves as a function of Ce^{3+} concentration. For the samples with higher Ce^{3+}concentrations ($x \ge 0.5$), the FC magnetization first increases sharply at T_N and then reaches a maximum and thereafter decreases with decreasing temperature (i.e., a broad maximum occurs in the FC mode). However, for the samples with lower Ce^{3+} concentrations ($x \le 0.4$), the FC magnetization, after a sharp rise at T_N, somewhat increases monotonically with decreasing temperature (i.e., with no signature of downturn). For samples with $x \ge 0.7$, the FC curves cross the ZFC curves. Remarkably, for $x \ge 0.8$, the FC magnetization becomes negative below ~70 K. A similar kind of behavior was observed in the $La_{1-x}Pr_xCrO_3$ sample.[20,21]

(19) Ong, K. P.; Blaha, P.; Wu, P. *Phys. Rev. B* **2008**, *77*, 073102.
(20) Yoshii, K.; Nakamura, A. *J. Solid State Chem.* **2000**, *155*, 447.
(21) Yoshii, K.; Nakamura, A.; Ishii, Y.; Morii, Y. *J. Solid State Chem.* **2001**, *162*, 84.

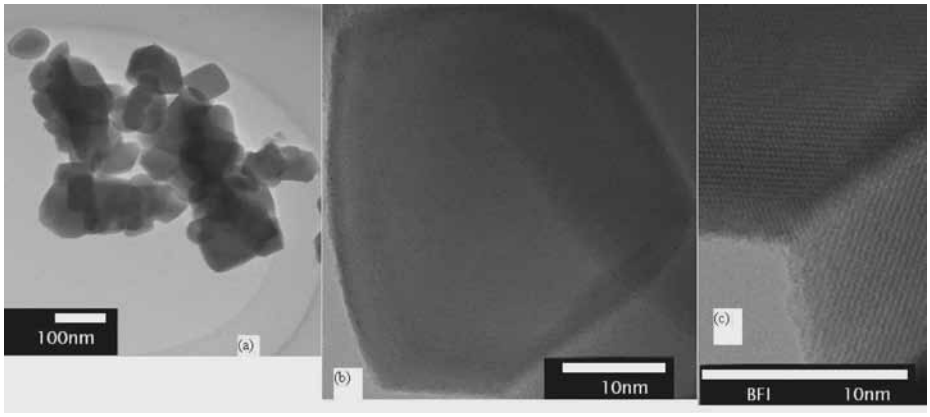

Figure 3. HR-TEM micrographs of $La_{0.5}Ce_{0.5}CrO_3$ as a typical case.

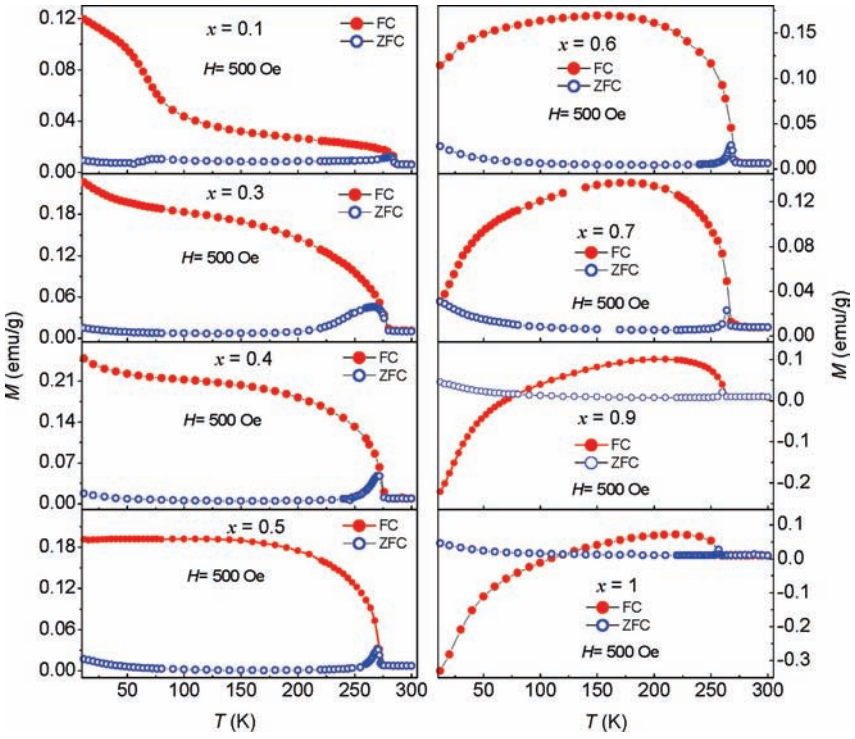

Figure 4. ZFC and FC magnetization as a function of temperature for $La_{1-x}Ce_xCrO_3$.

The observed magnetic behavior can be attributed to different ordering temperatures of the Cr^{3+} and Ce^{3+} ionic moments and their temperature dependency under an externally applied magnetic field in the presence of sublattice magnetocrystalline anisotropies. In the FC mode, when the Cr^{3+} sublattice moments order at T_N (~281.5−257 K) and get partially aligned along the applied magnetic field direction, a local internal magnetic field over the Ce^{3+} site is imposed. The Ce^{3+} sublattice, therefore, experiences a local field which is the vector sum of the internal field due to the Cr^{3+} sublattice and the external field (ca. $H = 500$ Oe) due to the field cooling. At a lower temperature, when the Ce^{3+} site gets ordered magnetically, the resulting magnetization of a sample can be derived from a superposition of the magnetizations of the Cr^{3+} and the Ce^{3+} sublattices. The relative contribution of the sublattices on the resultant magnetization depends on their individual temperature-dependent magnetic behaviors. Considering an AFM interaction between the Cr^{3+} and Ce^{3+} lattice site moments, the Ce^{3+} sublattice polarizes oppositely to the external magnetic field, and hence the total magnetization decreases with the ordering of the Ce^{3+} moment. For compounds with higher Ce concentrations, the Ce^{3+} sublattice magnetization becomes equal to the Cr^{3+} sublattice magnetization at the compensation temperature (T_{comp}). Upon further cooling, the Ce sublattice magnetization overcomes the Cr sublattice magnetization due to increased ordering of Ce^{3+} moments at lower temperatures, and the net magnetization becomes negative (i.e., aligned opposite to the applied magnetic field). However, the FC magnetization for compounds with a lower Ce concentration ($x \leq 0.4$) do not show any downturn with decreasing temperature, which implies that the effect of Ce sublattice magnetization in the resultant FC magnetization is negligible. However, the observed magnetic behavior in the ZFC mode can be explained qualitatively by assuming that both Cr^{3+} and Ce^{3+} sublattices are uncoupled as the samples are cooled under zero external field. In this case, the Ce moment does not get polarized, as the Cr site moments are orientated

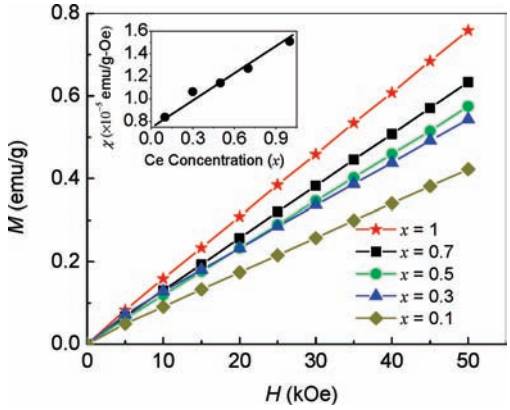

Figure 5. Magnetization as a function of applied field at 300 K for $La_{1-x}Ce_xCrO_3$ series.

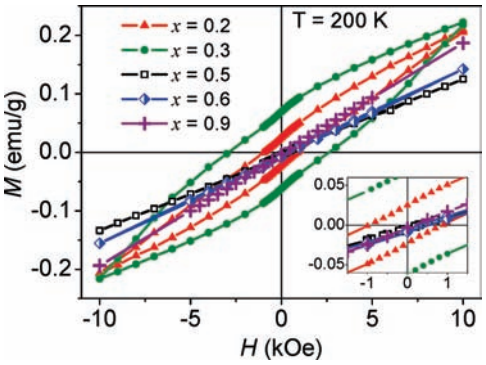

Figure 6. $M(H)$ curves at 200 K for $La_{1-x}Ce_xCrO_3$ series.

randomly. Therefore, both the sublattices contribute independently to the total magnetization.

Figure 5 shows the magnetization as a function of applied magnetic field [$M(H)$] at 300 K, that is, above the T_N. A linear behavior over the entire field range for all compounds, as expected for a typical paramagnetic material, is found. The inset shows the variation of the slopes of these $M(H)$ plots, that is, the mass susceptibility (χ) as a function of Ce^{3+} concentration. The χ increases linearly from 0.84×10^{-4} to 1.51×10^{-4} emu/g Oe with the increase of Ce^{3+} concentration from $x = 0.1$ to 1.0. The increase of paramagnetic susceptibility with the increase of Ce^{3+} content is attributed to the higher density of the unpaired electron ($4f^1$) in the series.

The $M(H)$ curves up to a maximum applied field of 10 kOe over all four quadrants at 200 K are shown in Figure 6 for some of the selected samples ($x = 0.2$, 0.3, 0.5, 0.6, and 0.9). A clear hysteresis has been observed for the samples with $x = 0.2$ and 0.3, however, with no tendency of saturation. On the other hand, the $M(H)$ curves for $x \geq 0.5$ samples do not show any hysteresis. The $M(H)$ curve for the $x = 0.9$ sample shows a linear field dependency, whereas a slight deviation from the linear behavior of $M(H)$ curves has been observed for $x = 0.5$ and 0.6 samples at this temperature. The observed small value of magnetization (0.22 emu/g = 0.0094 μ_B/f.u. for the $x = 0.3$ sample at 10 kOe field) and nonsaturation behavior of the $M(H)$ curves suggest the predominant AFM ordering (with a small canting for samples with $x \leq 0.5$) of Cr^{3+} spins. The canting of the Cr^{3+} spins increases initially with Ce substitution ($x \leq 0.3$) and then decreases with further Ce substitution and becomes zero for $x \geq 0.9$. In order to further

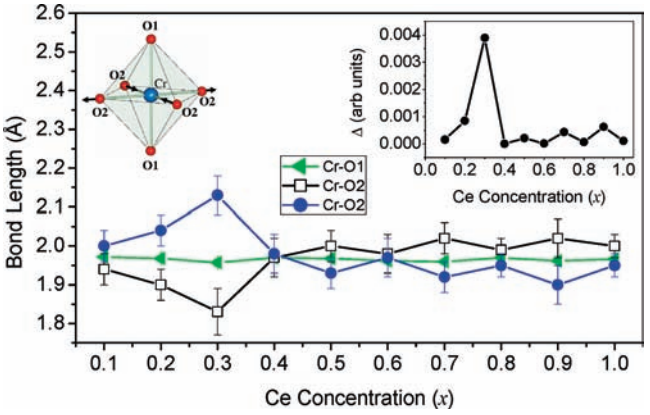

Figure 7. Cr−O bond lengths as a function of Ce concentration. Left inset shows the schematic diagram for expansion and contraction of Cr−O2 bond lengths in the basal plane of CrO_6 octahedra. Right inset shows the concentration-dependent distortion parameter (△) for CrO_6.

understand the magnetic properties of the $La_{0.1}Ce_{0.9}CrO_3$ sample, which shows negative magnetization, its hysteresis loop were recorded at several lower temperatures (10, 50, 100, and 200 K). The data are shown in the Supporting Information. An increase in the magnetization value was observed as a function of a decrease in the temperature. The overall behavior of the M versus H curve remains same throughout the temperature range.

To understand the origin of the canting of spins over the limited concentration range $0.1 < x \leq 0.3$ and magneto-structural coupling, we have done a detailed structural study at room temperature. Figure 7 shows the concentration dependence of the Cr−O bond lengths. A discrepancy in the basal bond lengths (Cr−O2) has been observed in the concentration range $0.1 < x < 0.4$ with a maximum at $x = 0.3$. Here, the bond length between Cr and two equivalent O2 ions (diagonally opposite) shows a peak (centered $\sim x = 0.3$), whereas the bond length between Cr and another two equivalent O2 ions shows a valley (centered $\sim x = 0.3$). However, the bond lengths between the Cr and apical O1 ions remain almost constant over all of the concentration range. Therefore, a distortion in the CrO_6 octahedra, an expansion along a diagonal, and a contraction along the other diagonal in the basal plane, occur in the concentration range $0.1 < x < 0.4$ (Figure 7). For further clarification, we have calculated the distortion parameter (△) of CrO_6 octahedra for all samples in this series according to the following equation:

$$\Delta = (1/6)\sum_{i=1}^{6}\{(d_i - < d >)/ < d > \}^2$$

where $< d >$ is the average bond length and d_i is the ith bond length. The value of △ as a function of Ce concentration has been plotted in the inset of Figure 7. With the substitution of Ce, the △ value increases initially and shows a maximum value of 0.00389 at $x = 0.3$. Upon further Ce substitution, the value of △ drops suddenly and remains almost constant over the remaining concentration range ($x \geq 0.4$). Interestingly, a weak ferromagnetic behavior was observed in our M(H) study for compounds $x = 0.2$ and 0.3. The observed weak ferromagnetic behavior due to the canting of the Cr spins may be attributed to the distortion in the CrO_6 octahedra.

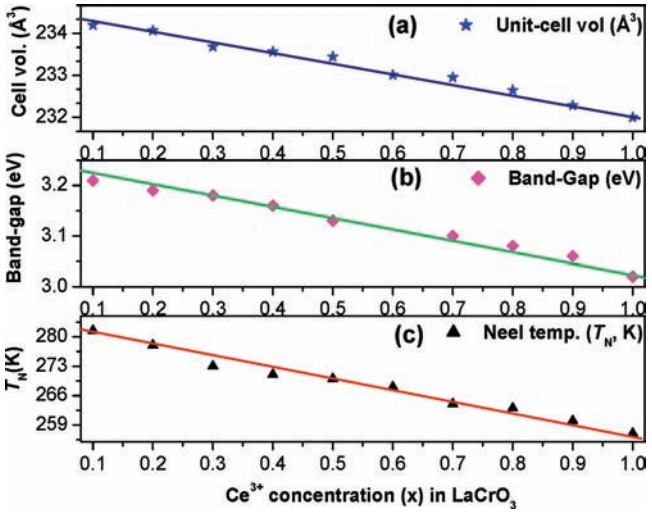

Figure 8. Ce^{3+} concentration (x) dependency of (a) unit-cell volume, (b) band-gap, and (c) Neel temperature, T_N, in $La_{1-x}Ce_xCrO_3$.

These detailed magnetic studies on $La_{1-x}Ce_xCrO_3$ compounds have revealed a very interesting as well as complex magnetization behavior. A detailed neutron diffraction investigation on individual compounds will reveal the exact origin of this complex magnetization.

The optical band gap in this new series of solid solutions measured as a function of Ce^{3+} concentration revealed a linear trend of decreasing band gap with the increase of Ce^{3+} concentration (from 3.21 eV for $x = 0.1$ to 3.02 eV for $x = 1$). Pure $LaCrO_3$ is known to be a wide band gap semiconductor with an optical band gap of 3.4 eV, which is considered to be a charge-transfer gap.[19] This is the energy gap between the top of the O_p bands at −2.0 eV and the bottom of the Cr^{3+} e_g conduction bands at 1.40 eV. The observed red shift as a function of Ce^{3+} content in $La_{1-x}Ce_xCrO_3$ is probably due to the decrease in the gap of O_p bands and Cr^{3+} e_g conduction bands, due to Ce^{3+} substitution. Thus, the present series of materials shows very fine-tuning to the band gap from the UV to visible region.

Figure 8a−c shows the variation of the unit cell volume, band gap, and Neel temperature as a function of Ce concentration in $La_{1-x}Ce_xCrO_3$. Remarkably, all of these properties show an exactly similar type of decreasing trend with increasing Ce^{3+} concentration. The unit cell volume decreases from 233.97(4) to 231.95(4) $Å^3$, the band gap decreases from 3.21 to 3.02 eV, and T_N decreases from 281.5 to 257 K with the increase of Ce^{3+} from $x = 0.1$ to 1.0. The substitution of Ce^{3+} for La^{3+} follows Vegard's law, as the lattice volume decreased linearly with increasing Ce^{3+} concentration. It has been observed for rare earth chromates that T_N decreases with decreasing rare-earth ion radius.[9] Our results are in accordance with this trend. This can be attributed to a decrease in average size of the A-site cation as a function the x value. Therefore, the different physical properties like optical and magnetic properties of these compounds are strongly coupled with their crystal structure.

Conclusion

Nanocrystalline $La_{1-x}Ce_xCrO_3$ ($0.0 \leq x \leq 1.0$) samples were successfully synthesized by a simple method involving two steps, namely, combustion followed by a vacuum heating. The formation of single-phase compounds of $La_{1-x}Ce_xCrO_3$ (over the entire range) was confirmed by an X-ray diffraction study as well as from other studies such as optical band gap and dc magnetization. Remarkably, these studies show a systematic decrease of the unit-cell volume, optical band gap, and T_N with increasing Ce^{3+} content. Thus, the new series of oxides prepared here exhibit the highly tunable band gap wherein its absorption shifts from UV to visible light, making it a potential material for photocatalysis. Similarly, the systematic shift in T_N from 281.5 to 257 K demonstrates the magnetic tunability of these oxides.

Acknowledgment. We sincerely acknowledge Mr. V. Rao of IIT-Bombay for band gap measurements.

Supporting Information Available: Rietveld refined atomic positions, isotropic thermal parameters, and different agreement factors for $La_{1-x}Ce_xCrO_3$ ($0.0 \leq x \leq 1.0$) and MH-loops at 10, 50, 100, and 200 K for $La_{0.1}Ce_{0.9}CrO_3$. This material is available free of charge via the Internet at http://pubs.acs.org.